ATR-FTIR Spectroscopy Studies of Iron−Sulfur Protein and Cytochrome c_1 in the *Rhodobacter capsulatus* Cytochrome bc_1 Complex[†]

Masayo Iwaki,[‡] Artur Osyczka,[§] Christopher C. Moser,[§] P. Leslie Dutton,[§] and Peter R. Rich*[,‡]

Glynn Laboratory of Bioenergetics, Department of Biology, University College London, Gower Street, London WC1E 6BT, U.K., and The Johnson Research Foundation, Department of Biochemistry and Biophysics, University of Pennsylvania, 1004 Stellar-Chance Building, 422 Curie Boulevard, Philadelphia, Pennsylvania 19104

Received April 20, 2004; Revised Manuscript Received May 28, 2004

ABSTRACT: Redox transitions in the *Rhodobacter capsulatus* cytochrome bc_1 complex were investigated by perfusion-induced attenuated total reflection-Fourier transform infrared (ATR-FTIR) spectroscopy combined with synchronous visible spectroscopy, in both the wild type and a cytochrome c_1 point mutant, M183K, in which the midpoint potential of heme was lowered from the wild-type value of 320 mV to 60 mV. Overall redox difference spectra of the wild type and M183K mutant were essentially identical, indicating that the mutation did not cause any major structural perturbation. Spectra were compared with data on the bovine bc_1 complex, and tentative assignments of several bands could be made by comparison with available data on model compounds and crystallographic structures. The bacterial spectra showed contributions from ubiquinone that were much larger than in the bovine enzyme, arising from additional bound and adventitious ubiquinone. The M183K mutant enabled selective reduction of the iron−sulfur protein which in turn allowed the IR redox difference spectra of ISP and cytochrome c_1 to be deconvoluted at high signal/noise ratios, and features of these spectra are interpreted in light of structural and mechanistic information.

The cytochrome bc_1 complex forms a superfamily of membrane-embedded enzymes that occur widely in eukaryotic and prokaryotic respiratory and photosynthetic electron transfer chains. A core complex encoded by *pet* genes consists of three subunits which are common to the superfamily: the "Rieske" iron−sulfur protein (ISP),[1] cytochrome c_1, and cytochrome *b*. These contain a 2Fe−2S cluster, a C heme, and two B hemes, respectively. This core catalyzes its ubiquinol-cytochrome *c* oxidoreductase and associated transmembrane proton transfer activities. Some bacterial forms have one additional small subunit, whereas the mammalian mitochondrial form can contain eight additional polypeptides.

Structures of several eukaryotic *bc* complexes have been determined at atomic resolution (*1*−*4*). The structures of the homologous cytochrome *bf* complex from cyanobacteria and green algae were also determined recently (*5*, *6*). It is widely agreed (*7*) that electron and proton transfer occurs by a "Q-cycle" mechanism (*8*). Ubiquinol oxidation at the "Q_o" binding site results in a concerted electron transfer in which the first electron is transferred to the ISP and the second to the lower-potential heme B, termed b_L. The electron on the ISP is passed via cytochrome c_1 to the substrate cytochrome *c*. The electron on heme b_L moves perpendicular to the membrane plane within the cytochrome *b* to reduce the higher-potential heme b_H. Reduced heme b_H reduces ubiquinone, which is bound at a second ubiquinone binding site termed Q_i, first to a bound, stabilized semiquinone and then with a second electron to ubiquinol. The Q-cycle provides a very efficient means of utilizing the energy of electron transfer to form a proton-motive force across the membrane.

The thermodynamic properties of the prosthetic groups are known and, together with the structures of the proteins, are in accord with expectations from the Q-cycle mechanism. However, some key details about the basic electron and proton transfer mechanism remain unclear, and this well-defined enzyme provides a useful experimental material in which to probe such basic questions. Particularly enigmatic are the chemical and physical factors that cause the strict bifurcation of electron transfer at the Q_o site (*9*−*11*). For example, questions about whether a remarkable long-range rotation of the globular protein domain of the ISP center is an essential feature for bifurcated electron transfer remain (*12*−*14*). Furthermore, on the basis of positions of various bound inhibitors, the Q_o site appears to be rather extensive. Other data on the EPR line shape of the ISP have indicated that two ubiquinones might be bound within the Q_o site (*15*), a suggestion supported by some inhibitor binding titrations (*16*) and more recently by NMR monitoring of ubiquinone displacement (*17*). These observations have led to proposals that two ubiquinols are required for functioning of the Q_o site (*18*) or that two sequential binding positions for ubiquinone species might be operative (*9*). Unfortunately, the Q_o site is not occupied by quinone substrate in available

[†] This work was funded by grants from the Wellcome Trust (Grant 062827) to P.R.R. and U.S. Public Health Service Grant GM-27309 to P.L.D.

* To whom correspondence should be addressed: Glynn Laboratory of Bioenergetics, Department of Biology, University College London, Gower Street, London WC1E 6BT, U.K. Telephone and fax: (+44) 020 7679 7746. E-mail: prr@ucl.ac.uk.

[‡] University College London.

[§] University of Pennsylvania.

[1] Abbreviations: ATR-FTIR, attenuated total reflection-Fourier transform infrared; ISP, Rieske iron−sulfur protein.

10.1021/bi049211x CCC: $27.50
Published on Web 07/02/2004

crystal forms, so this question remains unresolved. For both the Q_o and Q_i sites, and for the redox prosthetic groups, very little is known at present about which groups within the protein are specifically responsible for the extensive redox-linked protonation changes that are integral to the catalytic cycle.

Fourier transform infrared (FTIR) spectroscopy has been used extensively to probe structural changes in individual cofactors and amino acids in proteins. The first such studies on redox-induced changes were achieved by light-induced perturbation of photosynthetic reaction centers (*19*, *20*). Introduction of spectroelectrochemical cells allowed application of FTIR spectroscopy to redox changes in cytochrome *c* (*21*). Such methods, together with induction of redox changes with photochemicals, have since been extended to cytochrome *c* oxidase (*22*−*27*), complex I (*28*), and other redox proteins (*29*), providing information about modes of ligand binding, amino acid and prosthetic group changes, and protonation changes within the protein. Several FTIR studies of bc_1 complexes have appeared. Transmission FTIR in combination with thin-layer spectroelectrochemistry has been used to study the bacterial bc_1 complex (*30*, *31*). The bovine bc_1 complex has been analyzed by attenuated total reflection (ATR)-FTIR spectroscopy (*32*), and this procedure has provided the highest signal/noise data to date (*33*). This technique allows measurement of changes in the infrared spectrum of the sample while an aqueous solution is perfused over the sample surface and has already been applied to various proteins, including rhodopsin, bacteriorhodopsin (*34*), the nicotinic acetylcholine receptor (*35*), cytochrome oxidase (*36*−*38*), and reaction centers (*39*), and it greatly extends the types of transitions that can be analyzed by FTIR spectroscopy (*32*). Here we apply the method to the study of redox changes in thin layers of the *Rhodobacter capsulatus* cytochrome bc_1 complex that have been deposited on the surface of a silicon microprism. Both the wild type and a mutant form in which methionine serving as a sixth axial ligand to heme C in cytochrome c_1 is replaced with lysine (M183K) were studied. This mutation results in a large decrease in the midpoint redox potential of heme C, without affecting other parts or assembly of the complex (*40*), and has allowed accurate resolution of the IR redox difference spectrum of ISP from that of cytochrome c_1.

MATERIALS AND METHODS

Sample Preparation. Wild-type and mutant forms of the cytochrome bc_1 complex were isolated and purified from *Rba. capsulatus* as described in ref *41*. The *Rba. capsulatus* strain containing the M183K mutation was a generous gift from F. Daldal (University of Pennsylvania). Generation and properties of this mutant have been described in ref *40*.

Film Preparation. Production of stable films for ATR-FTIR measurements required depletion of detergent so that the sample became sufficiently hydrophobic. Film preparation and rehydration on a silicon microprism (3 mm diameter, three-bounce, SensIR Europe) with an "ATR-ready" enzyme were essentially as described previously (*42*). In brief, 10−20 μL of the cytochrome bc_1 complex (20−40 μM stock) was diluted in 20 mM potassium phosphate buffer (pH 7.5) containing 0.01% (w/v) sodium cholate and 0.01% (w/v) octyl glucoside and pelleted by centrifugation. The pellet was washed several times with the same buffer, and once with 2 mM phosphate buffer (pH 7.5). Finally, the ATR-ready detergent-depleted samples were dispersed into 10−20 μL of distilled water and stored if necessary at −80 °C.

A mixture of 2 μL of ATR-ready enzyme and 2 μL of distilled water was dried onto the prism and rehydrated with 200 μL of 100 mM *N*-(2-hydroxyethyl)piperazine-*N*′-2-ethanesulfonic acid (HEPES), 50 mM potassium phosphate, 100 mM KCl, and 50 mM K_2SO_4 (pH 7.5) (buffer A), and a Perspex chamber was placed over the sample to enable buffer flow and synchronous visible band spectroscopy as described in ref *33*. Perfusion buffers were either buffer A, 10 mM 2-(*N*-morpholino)ethanesulfonic acid (MES), 50 mM potassium phosphate, 100 mM KCl, 50 mM K_2SO_4 (pH 6.0), or 10 mM 2-(*N*-cyclohexylamino)ethanesulfonic acid (CHES), 100 mM potassium phosphate, 100 mM KCl, and 50 mM K_2SO_4 (pH 9.0). Other additions are described in the figure legends.

ATR-FTIR and Visible Spectroscopy. IR spectra were recorded with a Bruker IFS 66S spectrometer equipped with a liquid nitrogen-cooled MCT-A detector and a silicon ATR microprism (3 mm diameter, three reflections, SensIR Europe) as described in ref *32*. ATR-FTIR and visible difference spectra were recorded synchronously (*33*) as redox changes were induced by a change of the perfusant. Typically, a background spectrum (500 interferograms over 60 s) was recorded during the flow of the first buffer. The flow was then switched to the second buffer, and a sample spectrum (500 interferograms) was recorded. After this, a new background spectrum was recorded before the buffer was switched and a new sample spectrum was recorded. The process was cycled and repeated 20−100 times with two different films to obtain the final redox difference spectra. Corrections were made for any baseline drift due to protein swelling or shrinkage. IR spectra were measured with a resolution of 4 cm^{-1} and an accuracy of ± 1 cm^{-1}.

For measurements in deuterium oxide (D_2O), D_2O buffers at pD 7.5, prepared assuming $pD = pH_{reading} + 0.4$ (*43*), were substituted throughout the detergent depletion procedures. The extent of H−D exchange was estimated to be >90% using the method described in ref *44*. Redox cycles were repeated five to eight times to obtain the final spectra.

Analysis of Quinone Content. Ubiquinone was extracted with an acetone/methanol mixture and oxidized and purified following the method described in ref *45*. After being dissolved in 95% ethanol, it was quantitated from its reduced minus oxidized difference spectrum induced by reduction with potassium borohydride and using an extinction coefficient, ϵ, of 14 mM^{-1} cm^{-1} at 275 nm. The cytochrome bc_1 complex was quantitated from the concentration of total cytochrome *b* in a reduced minus oxidized difference spectrum using an ϵ of 28 mM^{-1} cm^{-1} at 560−574 nm (*46*), or from the concentration of cytochrome c_1 in an ascorbate-reduced minus ferricyanide-oxidized difference spectrum [ϵ = 19 mM^{-1} cm^{-1} at 551−540 nm (*47*)].

Combined Electrochemistry/ATR-FTIR Spectroscopy on Ubiquinone. Ubiquinone-50 was dissolved to 2 mg/mL in an 80% diethyl ether/20% ethanol mixture. Several microliters were placed on a silicon microprism and allowed to evaporate to dryness. The layer was then rehydrated first with distilled water, followed by exchange with 100 mM potassium phosphate or 100 mM KCl (pH 8.0) and with 0.5

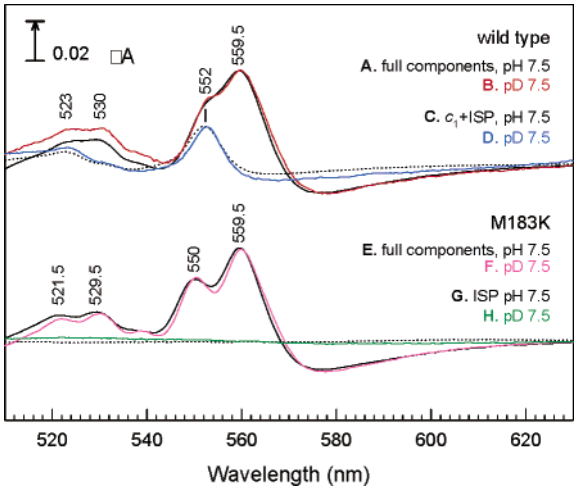

FIGURE 1: Perfusion-induced visible difference spectra of the *Rba. capsulatus* cytochrome bc_1 complex. Reduced minus oxidized visible difference spectra are shown for reduction and oxidation of all components (A and B for the wild type in H_2O and D_2O and E and F for the M183 mutant in H_2O and D_2O, respectively) or only high-potential components (C and D for the wild type in H_2O and D_2O and G and H for the M183 mutant in H_2O and D_2O, respectively). For redox changes of all components, a rehydrated film was perfused with a flow of buffer A (pH 7.5) containing 3 mM sodium dithionite. After 30 s, a background spectrum was recorded and the buffer was switched to buffer A containing 1 mM ferricyanide. After 30 s, the reduced minus oxidized difference spectrum was recorded. For redox change of high-potential components, buffer A was used with either 1 mM ferrocyanide with 100 μM hydroquinone or 1 mM ferricyanide. In all cases, data from five cycles were averaged to produce the spectra that are shown.

mM anthraquinone-2,6-disulfonate added as a redox mediator. An electrochemical cell (constructed in-house) was placed over the sample. This consisted of a 5 mm diameter glassy carbon working electrode approximately 0.5 mm above the prism that formed the top of a sample chamber approximately 50 μL in volume, connected via a salt bridge to a chamber with platinum counter and Ag/AgCl reference electrodes. An automated controller (constructed in-house) in conjunction with a PAR model 174A potentiostat allowed computer switching of the ambient potential of the sample mixture.

RESULTS

Perfusion-Induced Visible Difference Spectra. Perfusion-induced visible redox difference spectra are shown in Figure 1. For overall reduction and oxidation, the perfusant was alternated between buffer A (pH 7.5) containing either 3 mM sodium dithionite or 1 mM ferricyanide. The oxidation/reduction cycle was repeated five times, and spectra were averaged to produce the reduced minus oxidized difference spectra that are shown. A positive peak at 559.5 nm with a shoulder at 552 nm in the wild-type enzyme (traces A and B) and peaks at 559.5 and 550 nm in the M183K mutant (traces E and F) were observed in both H_2O and D_2O, consistent with the reported blue shift of the mutant cytochrome c_1 α-band (*40*).

Redox transitions of cytochrome c_1 and ISP alone were induced by alternation of buffer A containing 100 μM hydroquinone and 1 mM ferrocyanide with buffer A containing 1 mM ferricyanide. The ambient redox potential of the hydroquinone/ferrocyanide buffer was around 200 mV versus

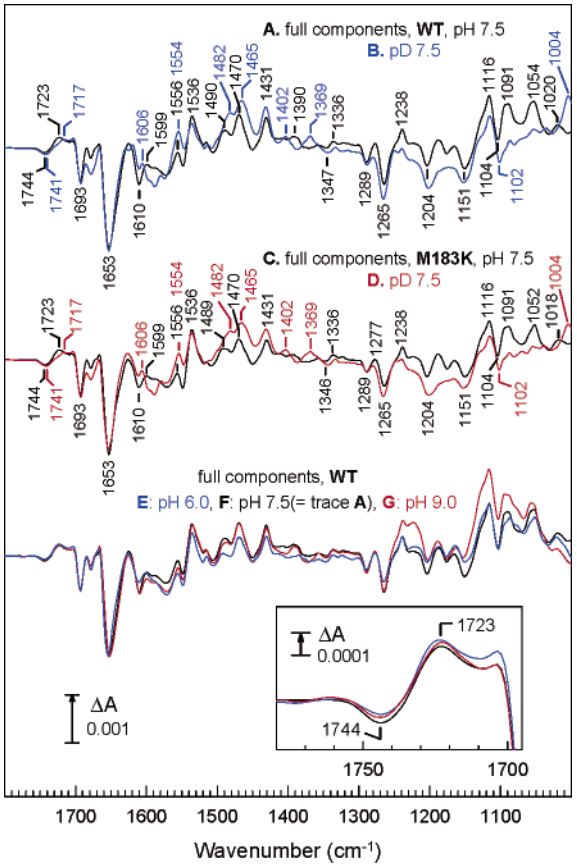

FIGURE 2: Perfusion-induced ATR-FTIR redox difference spectra of all components of the *Rba. capsulatus* cytochrome bc_1 complex. Reduced minus oxidized IR difference spectra are shown for reduction and oxidation of all components (A and B for the wild type in H_2O and D_2O and C and D for the M183 mutant in H_2O and D_2O, respectively). The bottom traces show an overlay of wild-type reduced minus oxidized IR difference spectra of all components in H_2O media at pH 6.0 (E), 7.5 (F, same as trace C), and 9.0 (G). ATR-FTIR difference spectra were recorded synchronously with visible spectra of samples shown in Figure 1. For each transition, a background spectrum was recorded (500 interferograms over 60 s), the buffer was changed, and an equivalent sample spectrum was recorded 30 s after exchanging the buffer. Spectra in H_2O and D_2O media are averages of 20 and 5 reductive/oxidative cycles, respectively. The inset shows expansions of the 1780−1695 cm^{-1} regions of traces E−G.

SHE, sufficient to fully reduce the cytochrome c_1 and ISP without reducing ubiquinone of the B hemes. In the wild-type enzyme, the visible difference spectra (Figure 1C) had a peak at 552 nm, demonstrating that cytochrome c_1 and, therefore, the roughly isopotential ISP were undergoing oxidation and/or reduction, whereas both B hemes remained unchanged. In the M183K enzyme, in contrast, practically no changes occurred in the visible region due to the lowered midpoint potential of cytochrome c_1 (trace G) (*40*). Similar results were obtained in H_2O media at pH 6.0 and 9.0 (not shown) and in D_2O media (traces D and H).

Overall Redox IR Difference Spectra. Redox-induced ATR-FTIR difference spectra were recorded concurrently with the visible difference spectra shown in Figure 1, although more cycles were averaged to produce an adequate signal/noise ratio. Figure 2 shows the corresponding IR difference spectra resulting from full oxidation or reduction of the bc_1 complex samples used in Figure 1. The reduced minus oxidized spectra shown are the average of 20 oxidized

minus reduced spectra inverted and averaged with 20 reduced minus oxidized spectra, and after subtraction of a baseline drift due to protein swelling or shrinkage. The reduced minus oxidized difference spectra of both the wild type and the M183K mutant in H_2O media (traces A and C) are very similar to each other, with principle features at 1744 (−), 1723 (+), 1693 (−), 1653 (−), 1556 (+), 1536 (+), 1490 (+), 1470 (+), 1431 (+), 1336 (+), 1289 (−), 1265 (−), 1238 (+), 1204 (−), 1151 (−), 1116 (+), 1104 (−), 1091 (+), 1054 (+), and 1020 cm^{-1}.

The effects of pH on the full reduced minus oxidized difference spectrum are shown in the bottom panel of Figure 2. All conditions of measurement were the same except for the buffer that was used. Overall, the major features remained remarkably similar over this pH range, and no significant variations of the shape or intensity of the 1744/1723 cm^{-1} trough/peak were observed (Figure 2, inset). However, a number of small but consistent changes were apparent and are discussed further below.

The redox difference spectra after H−D exchange are shown in traces B and D of Figure 2, obtained from an average of five redox cycles. The majority of bands remained unchanged. However, the 1744/1723 cm^{-1} trough/peak downshifted by 3−6 cm^{-1}, and the 1091, 1054, and 1020 cm^{-1} bands were absent. Downshifts of the 1490 and 1390 cm^{-1} peaks were also evident, and some small changes were also evident in the 1600 cm^{-1} region.

Individual Redox IR Difference Spectra of ISP and Cytochrome c_1. Reduced minus oxidized IR difference spectra of cytochrome c_1 with ISP in the wild-type enzyme in H_2O/D_2O media were recorded with the same samples used in Figure 1. Traces were the average of 100 redox cycles in H_2O or 8 in D_2O media, and baseline drifts due to protein swelling or shrinkage have again been subtracted from the spectra. The difference spectrum of the wild type in H_2O media (Figure 3A) had major bands at 1695 (−), 1669 (+), 1658 (−), 1643 (−), 1620 (+), 1535 (+), 1507 (−), 1494 (+), 1466 (+), 1448 (−), 1405 (+), 1212 (+), 1192 (−), 1116 (+), and 1101 (−) cm^{-1}. After H−D exchange, small bandshifts were observed in the 1685−1640 cm^{-1} amide I region with much larger effects in the 1570−1500 cm^{-1} amide II region, together with a number of other small changes discussed below (Figure 3B).

To extract redox IR difference spectra of ISP alone, the same redox reagents were used with the M183K mutant. In this case, only the ISP is expected to undergo redox changes since the midpoint potential of cytochrome c_1 is too low to be reduced by hydroquinone, which is confirmed by the lack of visible band changes in Figure 1. The resultant reduced minus oxidized difference IR spectra are shown in Figure 3C,D. In H_2O, major bands were present at 1695 (−), 1672 (+), 1658 (−), 1642 (+), 1617 (+), 1536 (+), 1508 (−), 1495 (+), 1447 (−), 1266 (+), 1214 (+), 1194 (−), 1135 (+), 1122 (−), 1107 (−), and 1095 (+) cm^{-1}. After H−D exchange, small alterations in the difference spectrum were observed in the amide I region with much larger effects in the amide II region.

Since these spectra should represent changes induced by redox changes solely of the ISP, subtractions of the difference spectra of the M183K mutant from those of the wild type result in reduced minus oxidized IR difference spectra of cytochrome c_1 alone (assuming that the spectra of ISP^- and

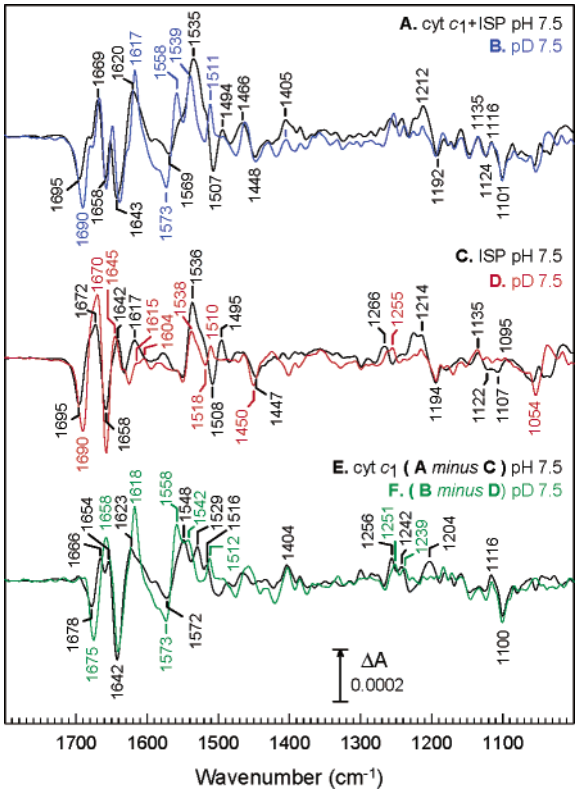

FIGURE 3: Perfusion-induced ATR-FTIR redox difference spectra of ISP and cytochrome c_1 of the *Rba. capsulatus* cytochrome bc_1 complex. Reduced minus oxidized IR difference spectra at pH 7.5 are shown for cytochrome c_1 with ISP in the wild type in H_2O (A) and D_2O (B), for ISP alone in the M183K mutant in H_2O (C) and D_2O (D). Calculated reduced minus oxidized IR difference spectra are shown for cytochrome c_1 alone in H_2O (E, trace A minus C) and D_2O (F, trace B minus D). ATR-FTIR difference spectra were recorded synchronously with visible spectra shown in Figure 1. For each transition, a background spectrum was recorded (500 interferograms over 60 s), the buffer was changed, and an equivalent sample spectrum was recorded 30 s after exchanging the buffer. Spectra in H_2O and D_2O media are averages of 100 and 8 reductive/oxidative cycles, respectively.

ISP are same in the wild type and M183K mutant). These calculated spectra in H_2O and D_2O media are spectra E and F of Figure 3, respectively. The spectrum in H_2O media has major bands at 1678 (−), 1666 (+), 1642 (−), 1623 (+), 1548 (+), 1529 (+), 1516 (+), 1404 (+), 1256 (+), 1242 (+), 1204 (+), 1116 (+), and 1100 (−) cm^{-1}. After H−D exchange, as for the spectra above, small bandshifts were observed in the amide I region with much larger effects in the amide II region, together with other small changes discussed below.

A further series of experiments identical to those with the M183K mutant were performed with the wild-type enzyme in the presence of 1 mM potassium cyanide in all perfusion media. Cyanide has been shown to bind to cytochrome c_1, lowering its midpoint potential significantly (*48*) and hence mimicking the effects of the M183K mutation. Visible difference spectra of the protein film agreed with those measured in solution (*48*). Redox IR difference spectra of ISP alone were essentially identical to those obtained in the M183K mutant in the absence of cyanide (data not shown). Hence, this control shows clearly that the effects of the M183K mutation are indeed localized to the heme C region

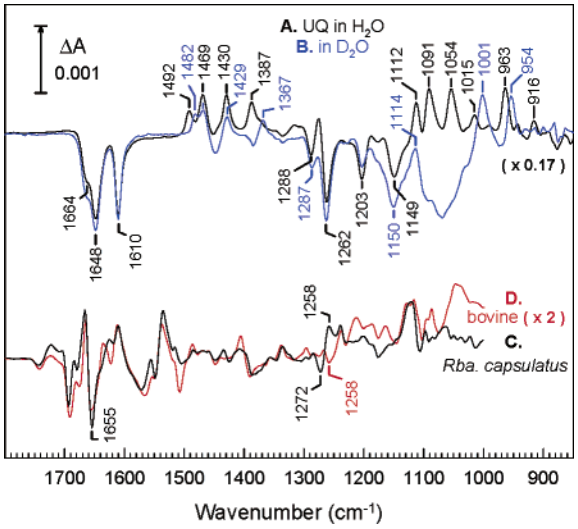

FIGURE 4: Redox IR difference spectra of ubiquinone-50 and comparison of redox difference spectra of *Rba. capsulatus* and bovine cytochrome bc_1 complexes. The ubiquinol minus ubiquinone difference spectra are averages of three 1000 IF scans vs the oxidized background in H_2O (A) or D_2O media (B), recorded as described in Materials and Methods. The bottom spectra (trace C) show the reduced minus oxidized IR difference spectrum of all components of the *Rba. capsulatus* cytochrome bc_1 complex (wild-type spectrum in H_2O of Figure 2A) after an interactive fractional subtraction of the redox difference of ubiquinone; i.e., the sum of trace A multiplied by 0.17 and trace C results Figure 2A. Overlaid on this is a normalized reduced minus oxidized IR difference spectrum of all components of the bovine mitochondrial cytochrome bc_1 complex (derived from data in Figure 3 of ref *33*).

with no additional alterations being induced in the ISP structure.

DISCUSSION

Perfusion-induced ATR-FTIR spectroscopy can provide data with a sufficient signal/noise ratio for identification of specific redox-induced atomic changes in large membrane proteins such as the cytochrome bc_1 complex studied here. The wide range of perfusants makes it possible to separate specific components of complex systems, and the ability to record synchronous visible band changes in the same sample provides a means of definitively associating specific IR features with individual redox components. By comparison with model compounds and by comparison with literature information on related proteins, preliminary assignments of several features of IR difference spectra are possible.

Overall Reduced minus Oxidized Spectra. Consistent with recent a recent transmission FTIR study of the bc_1 complex of *Paracoccus denitrificans* (*31*), the overall reduced minus oxidized IR redox difference spectra of the *Rba. capsulatus* enzyme are dominated by large signals that arise from ubiquinone and ubiquinol (refs *30* and *49* and Figure 2). This is clear if the spectra of Figure 2 are compared with redox difference spectra of ubiquinone-50 itself. Its electrochemically induced reduced minus oxidized difference spectra, shown in Figure 4, traces A (in H_2O) and B (in D_2O), both confirm and extend published spectra and assignments (*31*, *49*−*52*). Ubiquinone has no exchangeable protons, so its absolute spectrum is unaffected by H−D exchange. This can be seen from the lack of H−D sensitivity of the negative features of the redox difference spectra, all of which arise from ubiquinone. Troughs at 1664 and 1648 cm^{-1} have been assigned to the C═O stretching modes of quinone carbonyls, at 1610 cm^{-1} to the C═C ring bonds, and at 1288 and 1262 cm^{-1} to combination methoxy C−O/ring modes. Positive bands at 1492, 1469, 1430, 1387, 1112, 1091, 1054, and 1015 cm^{-1} can be assigned to ubiquinol formation. Since the protons of the ubiquinol hydroxyls are exchangeable, shifts on H−D exchange are expected and are indeed are seen in the 1492, 1387, 1091, 1054, and 1015 cm^{-1} bands, indicative of the contribution of the hydroxyl groups to these vibrational modes.

Equivalents of all of these bands, except for the 1664 cm^{-1} trough which is obscured by amide I changes, are seen in the redox IR difference spectra of the *Rba. capsulatus* bc_1 complex (Figure 2), and their similarity to free ubiquinone bands in terms of frequencies, relative intensities, and patterns of H−D shifts allows definitive assignment to ubiquinone (Table 1). However, when their magnitudes are compared to the magnitudes of the bands of the other prosthetic groups, these ubiquinone bands are 5−10 times larger than those observed in the bovine bc_1 complex, which has close to one ubiquinone per bc_1 complex, bound at the Q_i site (*33*). Equivalent bands have been observed in the *P. denitrificans* bc_1 complex previously and were also attributed to ubiquinone, in this case bound at the Q site(s) since the ubiquinone−bc_1 complex ratio was estimated to be close to 3 by comparison to IR spectra of free ubiquinone (*31*). To address the issue of their origin in the *Rba. capsulatus* enzyme, ubiquinone was extracted and quantitated from its UV redox difference spectrum, giving a ubiquinone−bc_1 complex monomer ratio of 6−8/1, consistent with the IR spectral intensities. Hence, although some of the ubiquinone is likely to be bound at one or both Q sites, the majority of the ubiquinone-related signals in our preparation can be attributed to adventitiously bound ubiquinone that remains attached to the preparation, a conclusion consistent with the similarity of the ubiquinone/ubiquinol bands with those of free quinone. Tentative assignments of IR bands of ubiquinone in cytochrome bc_1 complexes and in its free form are summarized in Table 1.

To compare the IR features of bc_1 complexes from *Rba. capsulatus* and bovine mitochondria more precisely, the dominating contributions of ubiquinone/ubiquinol were subtracted from the fully reduced minus oxidized difference spectrum of the bacterial bc_1 complex. Figure 4C shows the result after interactive fractional subtraction of the redox difference spectrum of ubiquinone (Figure 4A) from the redox difference spectrum of Figure 2A. The resulting ubiquinone-free redox difference spectrum (Figure 4C) is overall strikingly similar to the corresponding spectrum for the bovine enzyme (Figure 4D; replotted from ref *33*). A prominent trough at 1655 cm^{-1} in the amide I region, which was hidden by IR bands of ubiquinone, is clearly seen after subtraction. There are still some differences at 1272/1258 cm^{-1} that might arise because the environment of the adventitious ubiquinone results in slight bandshifts in comparison to the free ubiquinone spectra of Figure 4, resulting in slight inaccuracies in the subtraction process. Nevertheless, the comparison highlights the conservation of major IR features between these highly conserved structures once their differing ubiquinone contents are taken into account, and also shows that redox transitions of the

Table 1: Tentative Assignment of IR Bands[a] in Reduced minus Oxidized FTIR Spectra of Ubiquinone in the *Rba. capsulatus* Cytochrome bc_1 Complex

Rba. capsulatus, this work[b]		*Rba. capsulatus* electrochemistry, like Q_i[c]	*P. denitrificans* electrochemistry[d]	UQ, this work[e]		
H_2O	D_2O	H_2O	H_2O	H_2O	D_2O	assignment
1653 (−)	1653 (−)	1652 (−)	1656 (−)	1664/48 (−)	1664/48 (−)	quinone C═O
1610 (−)	1610 (−)	1608 (−)	1610 (−)	1610 (−)	1610 (−)	quinone C═C
1490 (+)	1482 (+)	1488 (+)	1494 (+)	1492 (+)	1482 (+)	quinol OH
1470 (+)	1465 (+)	1464 (+)	1468 (+)	1469 (+)	1469 (+)	quinol
1431 (+)	1431 (+)	1428 (+)	1430 (+)	1430 (+)	1429 (+)	quinol
1390 (+)	1369 (+)	1388 (+)	1388 (+)	1387 (+)	1367 (+)	methoxy Me
1289 (−)	1289 (−)	1284 (−)	1288 (−)	1288 (−)	1287 (−)	quinone methoxy/ring
1265(−)	1265 (−)	1262(−)	1262(−)	1262(−)	1262 (−)	quinone methoxy/ring
1204 (−)	1204 (−)	1202 (−)	1204 (−)	1203 (−)	1203 (−)	quinone methoxy/ring
1151 (−)	1151 (−)	1150 (−)		1150 (−)	1149 (−)	quinone methoxy/ring
1116 (+)				1112 (+)	1114 (+)	quinone methoxy/ring
1091 (+)	(<1000)			1091 (+)	<1000	quinol OH
1054 (+)	(<1000)			1054 (+)	<1000	quinol OH
1020 (+)	1004 (+)			1015 (+)	1001 (+)	quinol OH
				963 (+)	954 (+)	
				916 (+)		

[a] Peak positions in the reduced minus oxidized spectra are given in inverse centimeters. [b] From Figure 2A,B. [c] From Baymann et al. (*30*). [d] From Ritter et al. (*31*). [e] From Figure 4A,B.

adventitious ubiquinone do not result in additional IR band changes in the protein and prosthetic groups, again consistent with its nonspecific binding to the hydrophobic exterior of the complex.

The redox spectra exhibit a large 1744/1723 cm^{-1} trough/peak that most likely arises from C═O stretching modes of protonated aspartic and/or glutamic acids (*53*, *54*). These changes, which are essentially pH-independent between pH 6 and 9 (Figure 2), were not associated with the ISP−cytochrome c_1 redox difference spectra (Figure 3) and arise instead from redox changes of the B hemes and ubiquinone. A similar signal was found in equivalent spectra of the bovine bc_1 complex (Figure 4 and ref *33*), where it was shown to be composed of two components, one redox-linked to heme b_L and the other to heme b_H, tentatively ascribed to the conserved amino acids E272 and D229 (yeast numbering), residues that are located close to heme b_L and b_H, respectively (*1*−*4*). A similar feature has been observed in reduced minus oxidized difference spectra of the *P. denitrificans* bc_1 complex (*31*). However, in contrast to the bovine (*33*) and *Rba. capsulatus* systems (*30*), no changes at this position were present in the resolved redox difference spectra of the two hemes B alone, being replaced instead by a possible 1710 cm^{-1} band in heme b_H (*31*). Furthermore, emphasis was placed on small changes when the pH was varied between 5.5 and 7, in contrast to our data where such pH sensitivity is not evident. These authors suggested that the quinone content of their preparations was pH-dependent and that the shifts were linked to quinone bound in the Q sites (*31*). Hence, given these discrepancies, conclusions about the origin of the signals, its linkage to prosthetic groups, and its pH-dependent behavior should remain open until a more detailed analysis has been undertaken.

Despite the domination of the spectra overall by ubiquinone contributions, changes in the 1700−1620 and 1570−1500 cm^{-1} regions will inevitably contain changes in amide I and amide II bands, whereas other features can be assigned to vibrational changes of amino acid residues and specific redox cofactors. The deep troughs at 1693 and 1653 cm^{-1} are composed mainly of amide I changes from all redox components, of which the latter was overlapped by the ubiquinone carbonyl bands. The lack of significant H−D exchange effects on the 1556 and 1536 cm^{-1} bands suggests that this region cannot be dominated by amide II shifts and must contain other components, most likely from the heme groups themselves (cf. refs *29* and *55*). The H−D exchange-insensitive 1346/1336 cm^{-1} trough/peak and 1238 cm^{-1} peak are also typical of heme reduced minus oxidized difference spectra (*29*). A trough at 1104 cm^{-1} that is overlapped by the 1116 and 1091 cm^{-1} ubiquinol peaks most likely arises from histidine ligand(s) to the hemes (*56*).

Figure 2 (traces E−G) also shows an overlay of the overall reduced minus oxidized difference spectra at pH 6, 7.5, and 9. Remarkably, the overall pattern, including the 1740−1720 cm^{-1} carboxylic acid region discussed above, remains relatively constant over the pH range from 6 to 9, despite the fact that there are known redox-linked protonation changes with p*K* values within this range both for the B hemes and for the ISP (*11*). However, the redox spectra are dominated by ubiquinone/ubiquinol bands, which will not be expected to change over this pH range. pH-dependent bands associated with redox-linked amino acids will underlie these bands, and a detailed study of pH dependencies of spectra of deconvoluted components should provide insight into the key groups responsible for the known redox-linked protonation reactions.

Tentative Band Assignments for ISP. The use of selective reductants in combination with the perfusion ATR-FTIR technique (*33*) has allowed the separation of FTIR features associated with redox transitions of cytochrome c_1/ISP from cytochrome b_H/b_L and ubiquinone. By combining this technique with the use of the M183K cytochrome c_1 mutant, we have been able to selectively reduce the ISP alone and hence deconvolute very precisely the individual ISP and cytochrome c_1 IR redox difference spectra. This extends the frequency range, and with a considerably improved signal/noise ratio, in comparison to previous attempts to resolve these components by a combination of transmission FTIR,

Table 2: Tentative Assignment of IR Bands[a] in Reduced minus Oxidized FTIR Spectra of ISP in the *Rba. capsulatus* Cytochrome bc_1 Complex

Rba. capsulatus, this work[b]		*Rba. capsulatus* electrochemistry[c]	*P. denitrificans*, ISP fragment electrochemistry[d]	bovine[e]	
H_2O	D_2O	H_2O	H_2O	H_2O	tentative assignment
1695 (−)	1690 (−)	1692 (−)	1692 (−)	1691 (−)	amide I
1672 (+)	1670 (+)	1676 (+)			amide I
1658 (−)	1658 (−)	1656 (−)	1660 (−)		amide I
1642 (+)	1645 (+)	1646 (+)			amide I
1617 (+)	1614 (+)	1612 (+)		1610 (+)	amide I
1536 (+)	1538 (+)	1532 (+)	1536 (+)	1534 (+)	amide II
1508 (−)		1504 (−)		1507 (−)	Tyr
1495 (+)		1492 (+)			Tyr
1447 (−)	1450 (−)	1446 (−)		1464 (+)	
				1446 (−)	
1266 (+)	1255 (+)				
1214 (+)	1214 (+)				
1194 (−)	1194 (−)				
1135 (+)	1135 (+)				His
1122 (−)					His
1107 (+)					His
1095 (+)					His

[a] Peak positions in the reduced minus oxidized spectra are given in inverse centimeters. [b] From Figure 3C,D. [c] From Baymann et al. (*30*). [d] From Ritter et al. (*31*). [e] From Iwaki et al. (*33*).

spectroelectrochemistry, with global deconvolution algorithms (*30*), although the data presented here are roughly in accord with this previous study.

The IR redox difference spectra of the ISP are not expected to contain vibrational modes of the 2Fe−2S prosthetic group in the frequency range used here, since these are expected only below 800 cm^{-1}. Indeed, the major changes occur between 1695−1617 and 1536−1508 cm^{-1} and are likely to be dominated by amide I and amide II polypeptide backbone changes with other smaller changes elsewhere in the 2000−1000 cm^{-1} window. The large size of the trough at 1695 cm^{-1} in the amide I region is somewhat unusual, and has been observed consistently in other studies (*30*, *31*, *33*). An amide I C═O stretching band at this frequency is associated with backbone turns and bends (*57*). The bands at 1672 (+), 1658 (−), and 1642 (+) cm^{-1} can be assigned to amide I of β-sheets, turn/bends, and random coil, respectively. It is likely that changes in the conformation of the hinge region of the ISP that have been observed in crystallographically determined structures (*1*−*4*) will contribute to these amide I changes. Further comparison with the spectra of the isolated headgroup (cf. ref *31* and work in progress) should help in clarification of this point. However, the degree of H−D exchange sensitivity of this region is much greater than expected if the changes arose solely from amide I changes. Furthermore, the band at 1617 (+) cm^{-1}, which is missing after H−D exchange, is rather outside the amide I envelope. Hence, it seems likely that changes in H−D exchange-sensitive amino acids are also present within this region, possibly related to residues in the extensive salt bridge/hydrogen bond network of arginine and carboxylic acid residues that is present (*58*).

The peak at 1536 cm^{-1} is very sensitive to H−D exchange and is assigned to amide II shifts, consistent with assignment for the *Rba. capsulatus* ISP (*30*) and an ISP fragment of *P. denitrificans* (*31*). A rather sharper peak/trough can be seen at 1508 (−)/1495 (+) cm^{-1}. This region is typical of the tyrosine ring vibrational mode, and its downshift may arise from an environmental shift or ring hydroxyl deprotonation upon ISP reduction. The finding that both the peak and trough are lost in D_2O media would then have to arise from the downshift in D_2O of the 1508 cm^{-1} trough into the 1495 cm^{-1} peak (Table 2), causing them to cancel in the difference spectrum. The change at 1266 cm^{-1}, which is also present in the ISP headgroup (*31*), may be an additional feature of the same tyrosine. A candidate is Tyr185 whose hydroxyl group is hydrogen bonded to the sulfur of the iron-ligating Cys159 ligand (yeast numbering, Figure 5) (*58*). A trough at 1447 cm^{-1} was slightly upshifted upon H−D exchange and disappeared at low pH (not shown). A similar trough was assigned to a ring vibration of proline (P166 and/or P195,

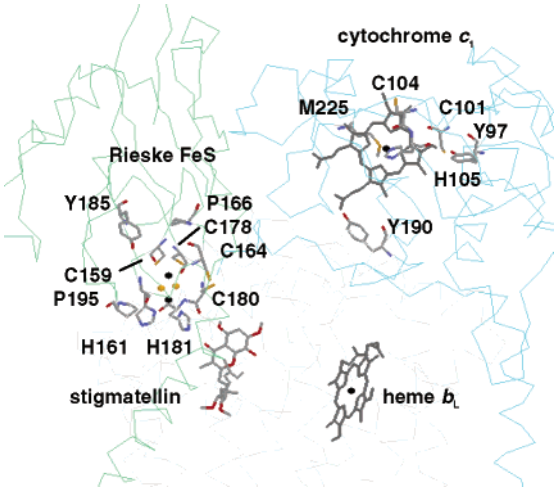

FIGURE 5: Some key conserved amino acid residues in the vicinity of the 2Fe−2S and heme C domains of the yeast cytochrome bc_1 complex. Selected amino acid residues and metal ligands that are candidates for redox-induced IR-detectable changes are highlighted (yeast sequence numbering). These residues are located within 7.0 Å of the surfaces of the 2Fe−2S and heme C prosthetic groups and are conserved in the *Rba. capsulatus*, bovine, and yeast sequences. Heme b_L and a stigmatellin molecule that occupies the Q_o site are also shown. Fe and S atoms in the metal centers are shown as black and purple dots, respectively. Atomic coordinates were taken from PDB entry 1KYO of the yeast cytochrome bc_1 complex (*61*).

Table 3: Tentative Assignment of IR Bands[a] in Reduced minus Oxidized FTIR Spectra of Cytochrome c_1 in the *Rba. capsulatus* Cytochrome bc_1 Complex

Rba. capsulatus, this work[b]		*Rba. capsulatus* electrochemistry[c]	*P. denitrificans*, c_1 fragment electrochemistry[d]	bovine, c_1 fragment[e]	
H_2O	D_2O	H_2O	H_2O	H_2O	tentative assignment
1678 (−)	1675 (−)		1682 (−)	1686 (−)	heme propionate
1666 (+)	1658 (+)	1666 (+)			amide I
1642 (−)	1642 (−)	1638 (−)	1644 (−)	1631 (+)	amide I
1623 (+)	1618 (+)	1612 (+)		1622 (−)	amide I, CαCβ heme
				1612 (+)	
1548 (+)	1558 (+)	1554 (+)		1558 (+)	CaCm/CbCb heme, amide II
1529 (+)	1542 (+)	1536 (+)	1534 (+)	1535 (+)	CbCb heme, amide II
1516 (+)	1512 (+)	1514 (+)			amide II
1404 (+)	1404 (+)	1402 (+)		1409 (+)	CaN heme
1256 (+)	1251 (+)				
1242 (+)	1239 (+)			1243	CmH heme
				1217 (+)	
1116 (+)	1116 (+)				His
1100 (−)	1100 (−)				His

[a] Peak positions in the reduced minus oxidized spectra are given in inverse centimeters. [b] From Figure 3E,F. [c] From Baymann et al. (*30*). [d] From Ritter et al. (*31*). [e] From Iwaki et al. (*33*).

yeast numbering) or tryptophan in *Rba. capsulatus* (*30*) and, although not noted, may also be in the corresponding spectrum of the *P. denitrificans* enzyme (*31*). Such assignment will require further studies.

X-ray crystal structures suggest that the globular headgroup of ISP can move between "*b*" and "c_1" positions to facilitate redox reaction with Q_o ubiquinol and cytochrome c_1, respectively (*1*−*4*). In the *b* position, the Nτ atom of H181 of ISP (yeast numbering) can form a hydrogen bond with a Q_o ubiquinol hydroxyl, whereas in the c_1 position, this residue may hydrogen bond with a free heme C propionate (*2*, *3*). It is quite possible that the distribution of the ISP headgroup between binding sites is dependent on the ISP redox state, with occupancy of the c_1 position expected to be favored when ISP is reduced and cytochrome c_1 is oxidized. Hence, some of the bandshifts in the ISP redox IR difference spectra may actually arise from cytochrome c_1 and/or the Q_o site and its bound ubiquinone occupant(s), induced by ISP headgroup redistribution. Features in the ISP redox IR difference spectra at 1214 (+) and 1194 (−) cm^{-1} are not frequencies that can be assigned to any known major amino acid vibrations. Comparison with the IR features of ubiquinone-50 (Figure 4) suggests the possibility that they could be associated with bandshifts of oxidized ubiquinone, caused by conformational strain, rather than redox changes, of the ubiquinone ring. A W-shaped feature at 1135 (+)/1122 (−)/1107 (−)/1095 (+) cm^{-1} may indicate perturbation of two histidine residues, H161 and H181 (yeast numbering), that ligate the iron atoms of the 2Fe−2S cluster through their Nπ atoms (*58*). According to theoretical predictions of Hasegawa *et al.* (*56*), an Nπ metal-ligated and Nτ-deprotonated form of 4-methylimidazole should exhibit a C5N1 stretching mode at 1132 cm^{-1}, whereas an Nπ metal-ligated and Nτ-protonated form should have a corresponding mode at 1094 cm^{-1}. These changes may be induced not only by ISP redox change but also by changes in binding to the Q_o site and cytochrome c_1. Further studies of this ISP signature in isolated components should help address this issue, and its pH dependency should provide a means of identification of protonation sites that are redox-linked to the 2Fe−2S cluster. Tentative assignments of the IR bands of ISP are summarized in Table 2.

Tentative Band Assignments for Cytochrome c_1. The M183K cytochrome c_1 mutant has also allowed the redox IR difference spectrum of cytochrome c_1 to be deconvoluted from that of ISP by subtraction of the ISP contribution from the spectrum of the wild type that can be attributed to both ISP and cytochrome c_1 together (Figure 3). An equivalent spectrum, albeit at a lower signal/noise ratio, has been achieved previously by combination of transmission FTIR, spectroelectrochemistry, and global deconvolution algorithms (*30*). In addition, redox IR difference spectra of the soluble globular domain of bovine (*33*) and *P. denitrificans* (*31*) cytochrome c_1 have been reported at rather low resolution. The deconvoluted spectra presented here are in general accord with these prior spectra.

The main features of the IR redox difference spectrum of cytochrome c_1 are again as expected concentrated in the amide I and II regions. These are dominated by troughs at 1678 and 1642 cm^{-1}, together with smaller overlapping bands, and a large amide II trough/peak at 1572/1548 cm^{-1}. However, whereas large H−D shifts are both expected and observed in the amide II region, significant changes also occur in the amide I bands where H−D shifts should be small. Hence, as for the ISP spectra, it seems probable that amino acid(s) that have strong H−D exchange-sensitive bands are also contributing in this region. Smaller features at 1529 and 1516 cm^{-1} and changes around 1404, 1256, and 1242 cm^{-1} occur in regions where redox-dependent heme bands should occur and, therefore, are likely to arise from the heme C itself. Again their pattern is roughly consistent with data of Baymann *et al.* (*30*) and with soluble cytochrome c_1 (*31*, *33*). Our spectra presented here extend data to 1000 cm^{-1} for the first time and show a deep trough at 1100 cm^{-1} that is H−D exchange-insensitive. This is characteristic for an Nτ metal-bonded histidine with a protonated Nπ position (*56*, *59*) whose environment is perturbed when the heme group undergoes redox change and is likely therefore to represent perturbation of the histidine heme ligand (H105 in yeast sequence numbering; Figure 5).

A further positive band at 1204 cm^{-1} that is absent after H−D exchange is also evident in the spectrum, though its origin is unknown at present. Tentative assignments of the IR bands of cytochrome c_1 are summarized in Table 3.

In contrast to ISP where there is strong sequence conservation around the prosthetic group, amino acid residues that surround heme C are not well-conserved between bacterial and mammalian forms, and since the bacterial bc_1 structure has not yet been determined, this limits the degree to which tentative assignments to specific residues can be made (see Figure 5). However, it is likely that a bacterial structure may soon be available (*60*), in which case a comparison of differences in redox IR spectra with differences in structures may aid further assignments.

In conclusion, we have determined individual redox-induced IR signatures of the ISP and cytochrome c_1 components of the *Rba. capsulatus* cytochrome bc_1 complex at high quality by using perfusion-induced ATR-FTIR spectroscopy combined with mutagenesis. The major features of the redox difference spectra of the components show reasonable consistency with prior data on bacterial and bovine enzymes and can in part be interpreted in terms of localized changes in cofactor and amino acids. The work now provides a basis for more detailed studies aimed at definition of redox-linked protonation events, domain movements of the ISP, and properties of the ubiquinone and ubiquinol substrates when bound in the two catalytic Q sites.

ACKNOWLEDGMENT

We thank Dr. Fevzi Daldal for a generous gift of the *Rba. capsulatus* strain containing the M183K mutation and Mr. Santiago Garcia for expert technical support.

REFERENCES

1. Xia, D., Yu, C.-A., Hoeon, K., Xia, J. Z., Kachurin, A. M., Zhang, L., and Deisenhofer, J. (1997) Crystal structure of the cytochrome bc_1 complex from bovine heart mitochondria, *Science 277*, 60−66.
2. Zhang, Z., Huang, L., Shulmeister, V. M., Chi, Y.-I., Kim, K. K., Hung, L.-W., Crofts, A. R., Berry, E. A., and Kim, S.-H. (1998) Electron transfer by domain movement in cytochrome bc_1, *Nature 392*, 677−684.
3. Iwata, S., Lee, J. W., Okada, K., Lee, J. K., Iwata, M., Rasmussen, B., Link, T. A., Ramaswamy, S., and Jap, B. K. (1998) Complete structure of the 11-subunit bovine mitochondrial bc_1 complex, *Science 281*, 64−71.
4. Hunte, C., Koepke, J., Lange, C., Rossmanith, T., and Michel, H. (2000) Structure at 2.3 Å resolution of the cytochrome bc_1 complex from the yeast *Saccharomyces cerevisiae* co-crystallized with an antibody Fv fragment, *Struct. Folding Des. 8*, 669−684.
5. Kurisu, G., Zhang, H., Smith, J. L., and Cramer, W. A. (2003) Structure of the cytochrome b_6f complex of oxygenic photosynthesis: tuning the cavity, *Science 302*, 1009−1014.
6. Stroebel, D., Choquet, Y., Popot, J.-L., and Picot, D. (2003) An atypical haem in the cytochrome b_6f complex, *Nature 426*, 413−418.
7. Berry, E. A., Guergova-Kuras, M., Huang, L.-S., and Crofts, A. R. (2000) Structure and function of cytochrome *bc* complexes, *Annu. Rev. Biochem. 69*, 1005−1075.
8. Mitchell, P. (1976) Possible molecular mechanisms of the protonmotive function of cytochrome systems, *J. Theor. Biol. 62*, 327−367.
9. Crofts, A. R., Barquera, B., Gennis, R. B., Kuras, R., Guergova-Kuras, M., and Berry, E. A. (1999) Mechanism of Ubiquinol Oxidation by the bc_1 Complex: Different Domains of the Quinol Binding Pocket and Their Role in the Mechanism and Binding of Inhibitors, *Biochemistry 38*, 15807−15826.
10. Jünemann, S., Heathcote, P., and Rich, P. R. (1998) On the mechanism of quinol oxidation in the bc_1 complex, *J. Biol. Chem. 273*, 21603−21607.
11. Osyczka, A., Moser, C. C., Daldal, F., and Dutton, P. L. (2004) Reversible redox energy coupling in electron transfer chains, *Nature 427*, 607−612.
12. Darrouzet, E., Moser, C. C., Dutton, P. L., and Daldal, F. (2001) Large scale domain movement in cytochrome bc_1: a new device for electron transfer in proteins, *Trends Biochem. Sci. 26*, 445−451.
13. Crofts, A. R., Guergova-Kuras, M., Huang, L.-S., Kuras, R., Zhang, Z., and Berry, E. A. (1999) Mechanism of ubiquinol oxidation by the bc_1 complex: role of the iron sulfur protein and its mobility, *Biochemistry 38*, 15791−15806.
14. Crofts, A. R., Hong, S., Zhang, Z., and Berry, E. A. (1999) Physiochemical Aspects of the Movement of the Rieske Iron Sulfur Protein during Quinol Oxidation by the bc_1 Complex from Mitochondria and Photosynthetic Bacteria, *Biochemistry 38*, 15827−15839.
15. Ding, H., Robertson, D. E., Daldal, F., and Dutton, P. L. (1992) Cytochrome bc_1 complex [2Fe-2S] cluster and its interaction with ubiquinone and ubihydroquinone at the Q_o site: A double-occupancy Q_o site model, *Biochemistry 31*, 3144−3158.
16. Brandt, U., Schägger, H., and von Jagow, G. (1988) Characterisation of binding of the methoxyacrylate inhibitors to mitochondrial cytochrome *c* reductase, *Eur. J. Biochem. 173*, 499−506.
17. Bartoschek, S., Johansson, M., Geierstanger, B. H., Okun, J. G., Lancaster, C. R. D., Humpfer, E., Yu, L., Yu, C.-A., Griesinger, C., and Brandt, U. (2001) Three molecules of ubiquinone bind specifically to mitochondrial cytochrome bc_1 complex, *J. Biol. Chem. 276*, 35231−35234.
18. Brandt, U. (1996) Bifurcated ubihydroquinone-oxidation in the cytochrome bc_1 complex by proton-gated charge-transfer, *FEBS Lett. 387*, 1−6.
19. Mäntele, W., Nabedryk, E., Tavitian, B. A., Kreutz, W., and Breton, J. (1985) Light-induced Fourier transform infrared (FTIR) spectroscopic investigations of the primary oxidation in bacterial photosynthesis, *FEBS Lett. 187*, 227−232.
20. Tabitian, B. A., Nabedryk, E., Mäntele, W., and Breton, J. (1986) Light-induced Fourier transform infrared (FTIR) spectroscopic investigations of primary reactions in photosystem I and photosystem II, *FEBS Lett. 201*, 151−157.
21. Moss, D., Nabedryk, E., Breton, J., and Mäntele, W. (1990) Redox-linked conformational changes in proteins detected by a combination of IR spectroscopy and protein electrochemistry. Evaluation of the technique with cytochrome *c*, *Eur. J. Biochem. 187*, 565−572.
22. Hellwig, P., Rost, B., Kaiser, U., Ostermeier, C., Michel, H., and Mäntele, W. (1996) Carboxyl group protonation upon reduction of the *Paracoccus denitrificans* cytochrome *c* oxidase: Direct evidence by FTIR spectroscopy, *FEBS Lett. 385*, 53−57.
23. Hellwig, P., Behr, J., Ostermeier, C., Richter, O.-M. H., Pfitzner, U., Odenwald, A., Ludwig, B., Michel, H., and Mäntele, W. (1998) Involvement of glutamic acid 278 in the redox reaction of the cytochrome *c* oxidase from *Paracoccus denitrificans* investigated by FTIR spectroscopy, *Biochemistry 37*, 7390−7399.
24. Lübben, M., and Gerwert, K. (1996) Redox FTIR difference spectroscopy using caged electrons reveals contributions of carboxyl groups to the catalytic mechanism of haem-copper oxidases, *FEBS Lett. 397*, 303−307.
25. Yamazaki, Y., Kandori, H., and Mogi, T. (1999) Effects of subunit I mutations on redox-linked conformational changes of the *Escherichia coli bo*-type ubiquinol oxidase revealed by Fourier-transform infrared spectroscopy, *J. Biochem. 126*, 194−199.
26. Lübben, M., Prutsch, A., Mamat, B., and Gerwert, K. (1999) Electron transfer induces side-chain conformational changes of glutamate-286 from cytochrome bo_3, *Biochemistry 38*, 2048−2056.
27. Hellwig, P., Soulimane, T., Buse, G., and Mäntele, W. (1999) Similarities and dissimilarities in the structure−function relation between the cytochrome *c* oxidase from bovine heart and from *Paracoccus denitrificans* as revealed by FT-IR difference spectroscopy, *FEBS Lett. 458*, 83−86.
28. Hellwig, P., Scheide, D., Bungert, S., Mäntele, W., and Friedrich, T. (2000) FT-IR spectroscopic characterization of NADH: ubiquinone oxidoreductase (complex I) from *Escherichia coli*: oxidation of FeS cluster N2 is coupled with the protonation of an aspartate or glutamate side chain, *Biochemistry 39*, 10884−10891.

29. Berthomieu, C., Boussac, A., Mäntele, W., Breton, J., and Nabedryk, E. (1992) Molecular changes following oxidoreduction of cytochrome b_{559} characterized by Fourier transform infrared difference spectroscopy and electron paramagnetic resonance: Photooxidation in photosystem II and electrochemistry of isolated cytochrome b_{559} and iron protoporphyrin IX-bisimidazole model compounds, *Biochemistry 31*, 11460−11471.
30. Baymann, F., Robertson, D. E., Dutton, P. L., and Mäntele, W. (1999) Electrochemical and spectroscopic investigations of the cytochrome bc_1 complex from *Rhodobacter capsulatus*, *Biochemistry 38*, 13188−13199.
31. Ritter, M., Anderka, O., Ludwig, B., Mäntele, W., and Hellwig, P. (2003) Electrochemical and FTIR spectroscopic characterization of the cytochrome bc_1 complex from *Paracoccus denitrificans*: Evidence for protonation reactions coupled to quinone binding, *Biochemistry 42*, 12391−12399.
32. Goormaghtigh, E., Raussens, V., and Ruysschaert, J.-M. (1999) Attenuated total reflection infrared spectroscopy of proteins and lipids in biological membranes, *Biochim. Biophys. Acta 1422*, 105−185.
33. Iwaki, M., Giotta, L., Akinsiku, A. O., Schägger, H., Fisher, N., Breton, J., and Rich, P. R. (2003) Redox-induced transitions in bovine cytochrome bc_1 complex studied by perfusion-induced ATR-FTIR spectroscopy, *Biochemistry 42*, 11109−11119.
34. Zscherp, C., Schlesinger, R., Tittor, J., Oesterhelt, D., and Heberle, J. (1999) In situ determinatin of transient pK_a changes of internal amino acids of bacteriorhodopsin by using time-resolved attenuated total reflection Fourier-transform infrared spectroscopy, *Proc. Natl. Acad. Sci. U.S.A. 96*, 5498−5503.
35. Baenziger, J. E., Miller, K. W., and Rothschild, K. J. (1993) Fourier transform infrared difference spectroscopy of the nicotinic acetylcholine receptor: evidence for specific protein structural changes upon desensitization, *Biochemistry 32*, 5448−5454.
36. Rich, P. R., and Breton, J. (2002) Attenuated total reflection Fourier transform infrared studies of redox changes in bovine cytochrome *c* oxidase: Resolution of the redox Fourier transform infrared difference spectrum of heme a_3, *Biochemistry 41*, 967−973.
37. Nyquist, R. M., Heitbrink, D., Bolwien, C., Wells, T. A., Gennis, R., and Heberle, J. (2001) Perfusion-induced redox differences in cytochrome *c* oxidase: ATR/FT-IR spectroscopy, *FEBS Lett. 505*, 63−67.
38. Iwaki, M., Breton, J., and Rich, P. R. (2002) ATR-FTIR difference spectroscopy of the P_M intermediate of bovine cytochrome *c* oxidase, *Biochim. Biophys. Acta 1555*, 116−121.
39. Iwaki, M., Andrianambinintsoa, S., Rich, P. R., and Breton, J. (2002) Attenuated total reflection Fourier transform infrared spectroscopy of redox transitions in photosynthetic reaction centers: comparison of perfusion- and light-induced difference spectra, *Spectrochim. Acta Part A 58*, 1523−1533.
40. Darrouzet, E., Mandaci, S., Li, J., Qin, H., Knaff, D. B., and Daldal, F. (1999) Substitution of the sixth axial ligand of *Rhodobacter capsulatus* cytochrome c_1 heme yields novel cytochrome c_1 variants with unusual properties, *Biochemistry 38*, 7908−7917.
41. Robertson, D. E., Ding, H., Chelminski, P. R., Slaughter, C., Hsu, J., Moomaw, C., Tokito, M., Daldal, F., and Dutton, P. L. (1993) Hydroubiquinone-cytochrome c_2 oxidoreductase from *Rhodobacter capsulatus*: Definition of a minimal, functional isolated preparation, *Biochemistry 32*, 1310−1317.
42. Iwaki, M., Puustinen, A., Wikström, M., and Rich, P. R. (2003) ATR-FTIR spectroscopy of the P_M and F intermediates of bovine and *Paracoccus denitrificans* cytochrome *c* oxidase, *Biochemistry 42*, 8809−8817.
43. Glasoe, P. K., and Long, F. A. (1960) Use of glass electrodes to measure acidities in deuterium oxide, *J. Phys. Chem. 64*, 188−190.
44. Rath, P., DeGrip, W. J., and Rothschild, K. J. (1998) Photoactivation of rhodopsin causes an increased hydrogen−deuterium exchange of buried peptide groups, *Biophys. J. 74*, 192−198.
45. Takamiya, K., and Dutton, P. L. (1979) Ubiquinone in *Rhodopseudomonas sphaeroides*. Some thermodynamic properties, *Biochim. Biophys. Acta 546*, 1−16.
46. Berden, J. A., and Slater, E. C. (1970) The reaction of antimycin with a cytochrome *b* preparation active in reconstitution of the respiratory chain, *Biochim. Biophys. Acta 216*, 237−249.
47. Wood, P. M. (1980) The interrelation of the two *c*-type cytochromes in *Rhodopseudomonas sphaeroides* photosynthesis, *Biochem. J. 192*, 761−764.
48. Osyczka, A., Moser, C. C., and Dutton, P. L. (2004) Novel cyanide inhibition at cytochrome c_1 of *Rhodobacter capsulatus* cytochrome bc_1, *Biochim. Biophys. Acta 1655*, 71−76.
49. Bauscher, M., and Mäntele, W. (1992) Electrochemical and infrared-spectroscopic characterization of redox reactions of *p*-quinones, *J. Phys. Chem. 96*, 11101−11108.
50. Burie, J.-R., Boussac, A., Boullais, C., Berger, G., Mattioli, T., Mioskowski, C., Nabedryk, E., and Breton, J. (1995) FTIR spectroscopy of UV-generated quinone radicals: Evidence for an intramolecular hydrogen atom transfer in ubiquinone, naphthoquinone, and plastoquinone, *J. Phys. Chem. 99*, 4059−4070.
51. Bauscher, M., Nabedryk, E., Bagley, K., Breton, J., and Mäntele, W. (1990) Investigation of models for photosynthetic electron acceptors: Infrared spectroelectrochemistry of ubiquinone and its anions, *FEBS Lett. 261*, 191−195.
52. Hellwig, P., Mogi, T., Tomson, F. L., Gennis, R. B., Iwata, J., Miyoshi, H., and Mäntele, W. (1999) Vibrational modes of ubiquinone in cytochrome bo_3 from *Escherichia coli* identified by Fourier transform infrared difference spectroscopy and specific ^{13}C labeling, *Biochemistry 38*, 14683−14689.
53. Mäntele, W. (1996) in *Biophysical Techniques in Photosynthesis* (Amesz, J., and Hoff, A. J., Eds.) pp 137−160, Kluwer Academic Publishers, Dordrecht, The Netherlands.
54. Barth, A. (2000) The infrared absorption of amino acid side chains, *Prog. Biophys. Mol. Biol. 74*, 141−173.
55. Moigne, C. L., Schoepp, B., Othman, S., Verméglio, A., and Desbois, A. (1999) Distinct structures and environments for the three hemes of the cytochrome bc_1 complex from *Rhodospirillium rubrum*. A resonance Raman study using B-band excitations, *Biochemistry 38*, 1066−1076.
56. Hasegawa, K., Ono, T.-A., and Noguchi, T. (2002) Ab initio density functional theory calculations and vibrational analysis of zinc-bound 4-methylimidazole as a model of a histidine ligand in metalloenzymes, *J. Phys. Chem. A 106*, 3377−3390.
57. Arrondo, J. L. R., Muga, A., Castresana, J., and Goñi, F. M. (1993) Quantitative studies of the structure of proteins in solution by Fourier-transform infrared spectroscopy, *Prog. Biophys. Mol. Biol. 59*, 23−56.
58. Iwata, S., Saynovits, M., Link, T. A., and Michel, H. (1996) Structure of a water soluble fragment of the "Rieske" iron−sulfur protein of the bovine heart mitochondrial bc_1 complex determined by MAD phasing at 1.5 Å resolution, *Structure 4*, 567−579.
59. Berthomieu, C., and Hienerwadel, R. (2001) Iron coordination in photosystem II: interaction between bicarbonate and the Q_B pocket studied by Fourier transform infrared spectroscopy, *Biochemistry 40*, 4044−4052.
60. Berry, E. A., and Huang, L.-S. (2003) Observations concerning the quinol oxidation site of the cytochrome bc_1 complex, *FEBS Lett. 555*, 13−20.
61. Lange, C., and Hunte, C. (2002) Crystal structure of the yeast cytochrome bc_1 complex with its bound substrate cytochrome *c*, *Proc. Natl. Acad. Sci. U.S.A. 99*, 2800−2805.

BI049211X